Impact of Forest-Elevated Turbulence Levels on Wind Farm Performance

Kazda, Jonas; Zendehbad, M.; Chokani, N.; Abhari, R. S.

Published in:
International Journal of Gas Turbine, Propulsion and Power Systems (JGPP)

Publication date:
2017

Document Version
Peer reviewed version

Impact of Forest-Elevated Turbulence Levels on Wind Farm Performance

M. Zendehbad*, J. Kazda, N. Chokani, R. S. Abhari

Laboratory for Energy Conversion
Department of Mechanical and Process Engineering
ETH Zurich, Zurich, Switzerland
*Email: zendehbad@lec.mavt.ethz.ch

ABSTRACT

This experimental work details the impact of forest-elevated turbulence levels on wind farm performance. In this regard, at two utility-scale wind farms, one in flat forested terrain and the second in flat unforested terrain, measurements of the wind flow field are made and the power performance of the wind turbines are assessed. A mobile scanning LiDAR system is used to make measurements of the wind speed and turbulence intensity both in the freestream and downstream of a forest. Turbulence intensities up to 26% are measured immediately downstream of the forest at hub height, whereas in the freestream the turbulence intensity does not exceed 15%. While the turbulence levels decay as the wind flow evolves downstream, even at a downstream distance of 20 times the forest height, the turbulence intensities are above the freestream turbulence intensities. On the other hand the deficit in wind speed that is measured immediately downstream of the forest is negligible at a downstream distance of 15 times the forest height. A comparison of the power performance of wind turbine without and with a forested fetch is made. It is shown that with a forested fetch there is a 30% loss in performance due to the forest-affected wind flow. An assessment of the power production of the individual wind turbines in the two wind farms is made to assess the impact of forest-elevated turbulence levels on wake losses. It is seen that the wake losses are lower in forested terrain compared to unforested terrain.

Nomenclature

a_{11}, a_{22}, a_{33}	coefficients on diagonal of turbulence stress tensor
D	rotor diameter
H_{forest}	height of forest
u', v', w'	wind speed fluctuations in principal, lateral and vertical wind direction.
u^*	turbulence friction velocity
u_{ref}	time-averaged horizontal wind speed at each range gate
$\sigma_x, \sigma_y, \sigma_z$	wind speed standard deviation in principal, lateral and vertical wind direction.
τ_{ij}	turbulence stress tensor component, where i, j is x, y or z
θ	laser beam elevation angle
ρ	density

Abbreviations

AEY	annual energy yield
AGL	above ground level
CFD	computational fluid dynamics
DA	degree of anisotropy
IEC	International Electrotechnical Commission
LES	large eddy simulation
LiDAR	light detection and ranging
LOS	line-of-sight
PSD	power spectral density
RANS	Reynolds-averaged Navier-Stokes
SCADA	supervisory control and data acquisition system
TI	turbulence intensity
TKE	turbulent kinetic energy
VAD	velocity azimuth display

INTRODUCTION

The cumulative installed wind capacity in Japan reached 2789MW in 2014, 98% of which is installed onshore [1]. Following the 2011 Fukushima disaster Japan's wind industry is expected to grow at a faster pace. 67% of Japan's land area is covered by forests [2]. As 54% of the remaining non-forested land are built-up areas [3] and due to regulations on the siting of wind farms in urban areas [4], an improved understanding of the impact of forests on the wind resource is required in order to effectively advance the development of onshore wind farm projects.

Field measurements show that the effect of forests extends as high as 5 times the forest height and as far as 500m downstream of a forest [5]. Meteorological mast measurements above the forest canopy show negligible difference in turbulence anisotropy upstream and downstream of forest edges [6-7]. Shear generation above the forest canopy is suggested to be the principal source of turbulence generation above and below the canopy, as TKE in the sub-canopy layer is observed to be one-tenth of TKE above the canopy [8]. In addition to full-scale experiments, sub-scale models [9] and CFD simulations [10-11] have investigated turbulence generation above and downstream of forests. LES simulations [10] show the presence of complex vorticity structure above the canopy, initiating from $9H_{forest}$ downstream of the forest edge. RANS simulation of flow over complex forest geometries were performed in [11], where TKE as high as twice the freestream TKE was computed downstream of the forest. Although numerous researchers have addressed the impact of forests on the wind flow above and downstream of forests, the impact of elevated turbulence levels on wind turbine's operation and power generation is not yet fully understood. The impact of elevated turbulence on turbine performance has been investigated in [12] using a sub-scale wind tunnel model. However in addition to a Reynolds number mismatch, the use of stiff models of forest trees is a concern since, the top of the forest canopy vibrates; these vibrations, and their attendant vorticity generation, are absent in the sub-scale experiment.

The present work details measurements upstream and downstream of full-scale forests. Furthermore the impact of forests on the energy yield of wind farms is assessed. In this regard the paper is organised as follows: first, details of the measurement sites and procedure are described. Second, the wind flow fields and wind turbine energy yields are compared for wind turbines downstream of a forest and downstream of an unforested flat-fetch. The paper concludes with the key observations.

METHODOLOGY

Mobile scanning LiDAR system

A scanning LiDAR system (Galion long range inland model) is used to measure the LOS component of wind speed. The measurement principle is based on the Doppler shift of backscattered laser light from aerosols in the atmosphere. The measurement accuracy is 0.05m/s to 0.10m/s [13] with a maximum range of 6km. The laser pulse rate is 15kHz with a measured energy per pulse of 5μJ. The LiDAR has a 3D scanning head that allows for volumetric scanning with an accuracy of 0.1° over 0° – 360° in the azimuth and -17° to 90° in elevation; the angular accuracy has been verified using an electronic spirit level (DIGILEVEL, Laserliner) whose accuracy is 0.1°. The LiDAR system is installed in a mobile laboratory, windRoverII, Fig. 1. This mobile laboratory is a vehicle equipped with a 5kW generator and a battery bank to provide electric power for the laboratory's on-board systems. During measurements the LiDAR scanning head is raised through an opening in the roof of windRoverII by an elevator. windRoverII can accommodate a two person crew for off-road measurement campaigns.

Fig. 1 Photograph of the mobile laboratory windRoverII that is equipped with the scanning LiDAR system. The LiDAR system is deployed through the roof of windRoverII.

Measurement sites

In this work, the measurements at two wind farms are presented. Measurements upstream and downstream of a forest are made at Wind Farm 1, Fig. 2; this 28MW wind farm is located in the flat terrain of eastern Germany. The wind farm is comprised of fourteen 2MW Vestas V80 wind turbines. All turbines have an 80m rotor diameter. The turbines measured at in this work, WEA10, WEA12, WEA13 and WEA14, have hub height of 78m AGL. The turbine cut-in and rated wind speeds are 4m/s and 14m/s, respectively. The land cover and surface elevation maps are shown in Fig. 2a and Fig. 2b, respectively. There are forests, with an average height of 40m AGL along the southern and eastern sides of the wind farm and a forest with an average height of 20m AGL along the northern and north-western sides of the wind farm. The land cover along the west side of the wind farm is mostly agricultural land. The forest of interest, whose downstream wind flow field is detailed in this work, is shown with the yellow dashed oval in Fig. 2a. It can be seen that the wind turbines are located in flat terrain at an elevation of 70m above sea level, Fig. 2b.

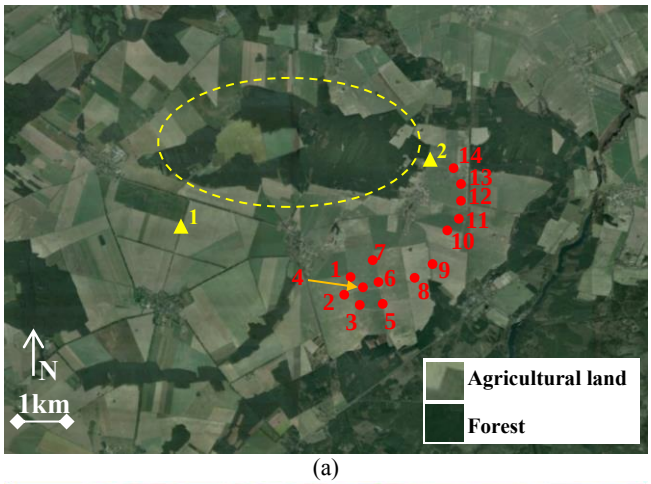

(a)

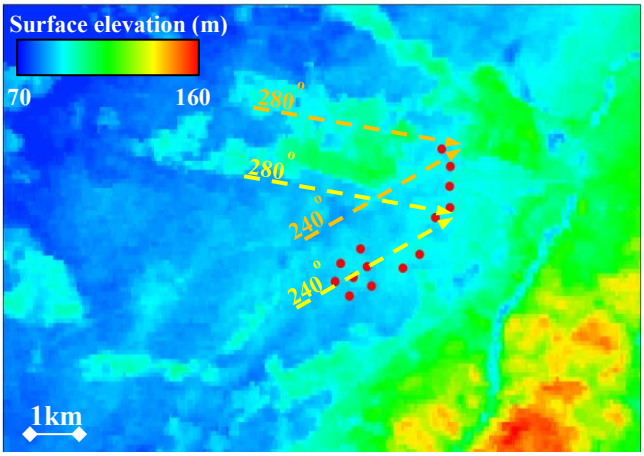

(b)

Fig. 2 Layout of the 28MW wind farm that is located in flat terrain in eastern Germany. a) map of land cover; the locations of the wind turbines are shown by the filled red circles. The respective turbine identification numbers examined in this work are shown. The prefix "WEA" is omitted from the numbers for the sake of brevity. The dashed yellow oval shows the forest of interest. The yellow triangle symbols show the measurement positions in the freestream ("1") and downstream of the forest ("2"). b) map of surface elevation; wind directions of interest, 240° to 280°, are shown by the dashed lines.

With a westerly wind direction as in the present work, this forest extends longitudinally up to 2.8km ($140H_{forest}$) upstream of the measurement position "2" and is 1.7km ($85H_{forest}$) wide in the lateral direction. The wind rose at the wind farm derived from one-year measurements by SCADA system of wind turbines is shown in Fig. 3. It is observed that the dominant wind directions are west, south-west and east. Wind directions of interest, between 240° and 280°, which are discussed below, have the highest occurrence of 27%.

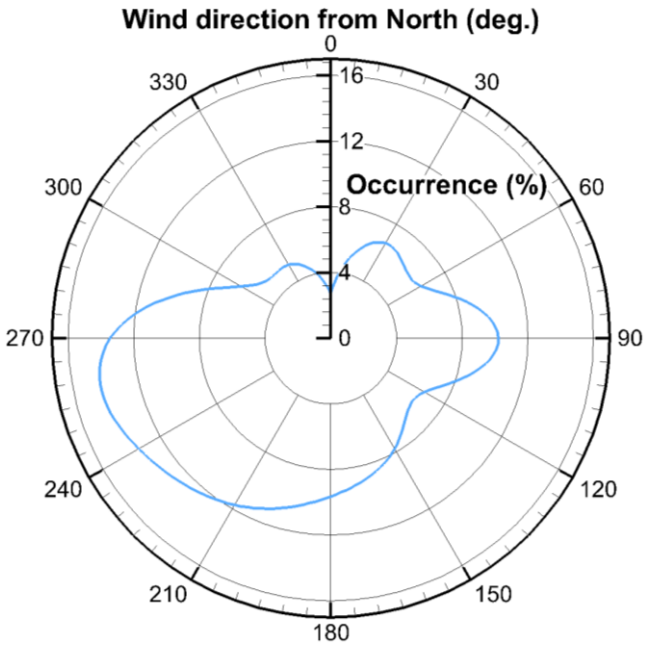

Fig. 3 Wind rose at Wind Farm 1.

In order to investigate the impact of forests on the wake recovery downstream of turbines, a one-year-long time series of SCADA data from Wind Farm 1 and a second wind farm were assessed. The second wind farm, Wind Farm 2, is located in flat coastal terrain in northern Germany. Wind Farm 2, shown in Fig. 4, is a 25.8MW wind farm that is comprised of nine wind turbines as detailed in Table 1.

Turbine no.	Rated power	Rated power	Rotor diameter	Hub height
1, 3, 5	Siemens SWT3.6	3.6MW	107m	93m
2, 4, 6	Vestas V90	3MW	90m	105m
7, 8, 9	Vestas V80	2MW	80m	60m

Table. 1 Characteristics of wind turbines located in Wind Farm 2. The wind turbine numbers are shown in Fig. 4b.

Fig. 4a and Fig. 4b show maps of the land cover at Wind Farm 2. The farm is located on agricultural land and is 3km and 6.5km away from the sea on its northern and western sides, respectively. Except for a sparse forest, which is 2km away on the western side, this wind farm is surrounded by flat unforested terrain. Fig. 4c shows the surface elevation map at the wind farm. The most salient feature is the forests on the west side whose heights vary from 20m AGL to 50m AGL.

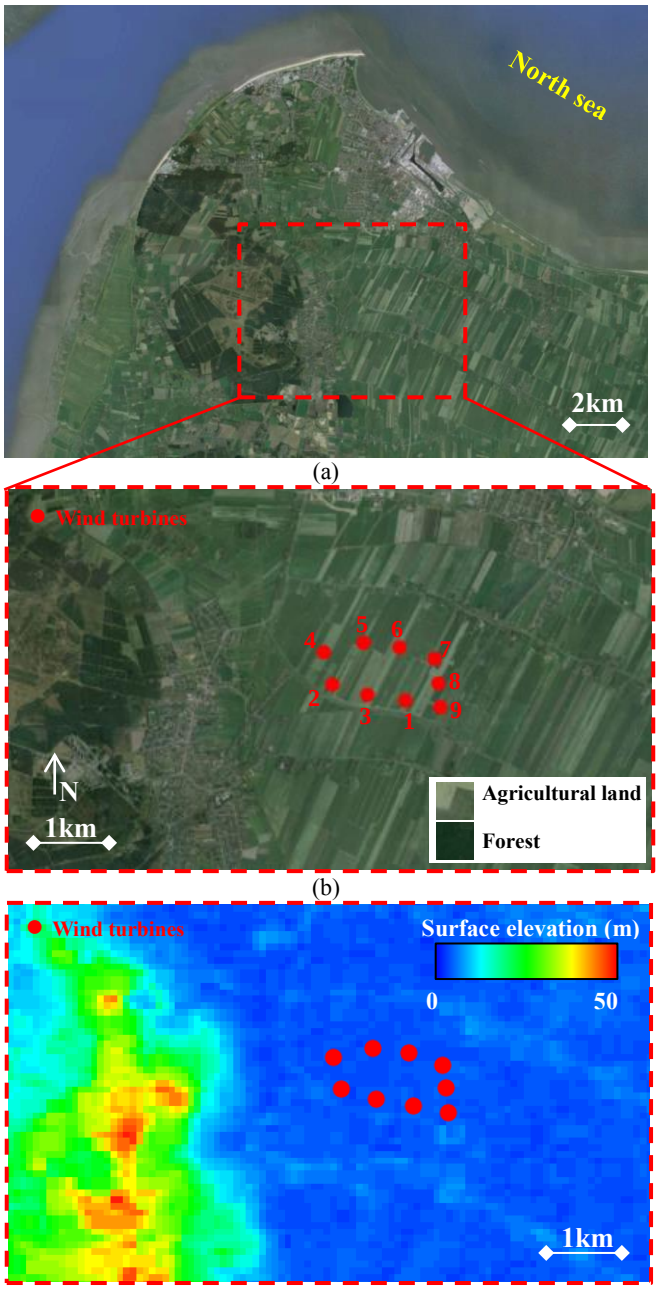

Fig. 4 Layout of 25.8MW wind farm that is located in flat coastal terrain in northern Germany; a) location of wind farm, the dashed red rectangle is detailed in Fig. 4b, b) map of land cover; the locations of the wind turbines are shown by the filled red circles. The respective turbine identification numbers are shown. The "WEA" prefix is omitted from the numbers for the sake of brevity, c) map of surface elevation.

Measurement procedure

The measurements of the wind field are made at Wind Farm 1, with winds from the west to east. Reference measurements are made in the freestream, position "1" in Fig. 2a. These freestream measurements are comprised of three 10-minute stare measurements and VAD scans. The stare measurements are made at elevation angles of 0^o, 18^o and 36^o, staring in the downstream direction. The VAD scans are made in order to measure vertical profiles of wind speed and direction. Measurements are also made downstream of the forest, position "2" in Fig. 2a, where stare scans with elevation angles of 0^o, 18^o and 36^o towards the downstream direction are made.

Data processing

The turbulence intensity is derived from LiDAR measurements in a stare scanning mode; that is measurement of LOS wind speed along a fixed direction. For these measurements, a 10-minute time series was sampled from 15 range gates at a frequency of 0.9Hz with a spatial resolution of 30m in the LOS direction.

The time series of measured wind speed data are filtered based on the signal-to-noise ratio. Local interpolation in time is used to estimate filtered out wind speeds. The turbulence intensity is given as:

$$TI = \frac{\sqrt{\frac{1}{3}\left(\overline{u'^2} + \overline{v'^2} + \overline{w'^2}\right)}}{u_{ref}} \quad (1)$$

Since the LOS wind speed is measured, the degree of turbulence anisotropy is used to bound the range of turbulence intensity.

The Degree of Anisotropy, DA, is given as:

$$DA = \frac{2\overline{u'^2}}{\overline{v'^2} + \overline{w'^2}} \quad (2)$$

The industry standard IEC 61400-1 [14], specifies standard deviations in the three directions as:

$$\frac{\sigma_y}{\sigma_x} = \left(\frac{\tau_{yy}}{\tau_{xx}}\right)^{0.5} = 0.8$$
$$\frac{\sigma_z}{\sigma_x} = \left(\frac{\tau_{zz}}{\tau_{xx}}\right)^{0.5} = 0.5 \quad (3)$$

which yields a DA of 2.25. Measurements at ETH Zurich using a nacelle-mounted probe [15] and a kite-based probe [16], as well as other atmospheric measurements [17-19], report DA in the range of 0.8 to 2.28. This range is used to estimate the expected range of turbulence intensities based on the turbulence intensity derived from the measurements of the LOS wind speed. In this regard, for different DA, the wind speed fluctuations in the LOS direction are related to the wind speed fluctuations in the principal wind directions using:

$$\sigma_u = \frac{\sigma_{u,LOS}}{\sqrt{\cos^2\theta + \left(\frac{\tau_{zz}}{\tau_{xx}}\right)\sin^2\theta + 2\left(\frac{\tau_{xz}}{\tau_{xx}}\right)\cos\theta sin\theta}} \quad (4)$$

in which the components of the turbulence stress tensor are given as:

$$\begin{bmatrix} \tau_{xx} & \tau_{xy} & \tau_{xz} \\ \tau_{yx} & \tau_{yy} & \tau_{yz} \\ \tau_{zx} & \tau_{zy} & \tau_{zz} \end{bmatrix} = \begin{bmatrix} a_{11}\rho u^{*2} & 0 & \rho u^{*2} \\ 0 & a_{22}\rho u^{*2} & 0 \\ \rho u^{*2} & 0 & a_{33}\rho u^{*2} \end{bmatrix} \quad (5)$$

As the coefficients along the diagonal of the stress tensor are a function of DA, σ_u is calculated from Equ. 4, and the turbulence intensity, given in Equ. 1, is calculated as:

$$TI = \frac{\sigma_u\sqrt{\frac{1}{3}\left[1 + \left(\frac{\tau_{yy}}{\tau_{xx}}\right) + \left(\frac{\tau_{zz}}{\tau_{xx}}\right)\right]}}{u_{ref}} \quad (6)$$

RESULTS AND DISCUSSION

Forest measurements

Fig. 5 shows the vertical profiles of wind speed and wind direction that are measured at position "1" that is shown in Fig. 2a. The error bars show the standard deviation during the measurement period. The height above ground level is normalised with respect to the forest height of 20m. The vertical profile of wind speed on a semi-log plot, Fig. 5b, is concave downwards, indicating that the atmospheric boundary layer is stable [20]. The wind speed monotonically increases from 4m/s at Z=2.5H_{forest} (50m AGL) up to 7.6m/s at Z=13.5H_{forest} (270m AGL). Fig. 5c, shows a westerly wind with a constant wind veer towards the east of 12° per 100m in height; this veer is in the same direction as the Coriolis force.

Fig. 6a shows the measured wind speed downstream of the forest. The wind speeds are normalised by the freestream wind speed at the corresponding height. The forest edge is at X=0 and the wind direction is from left to right. The LOS wind speeds are averaged over 10-minute windows.

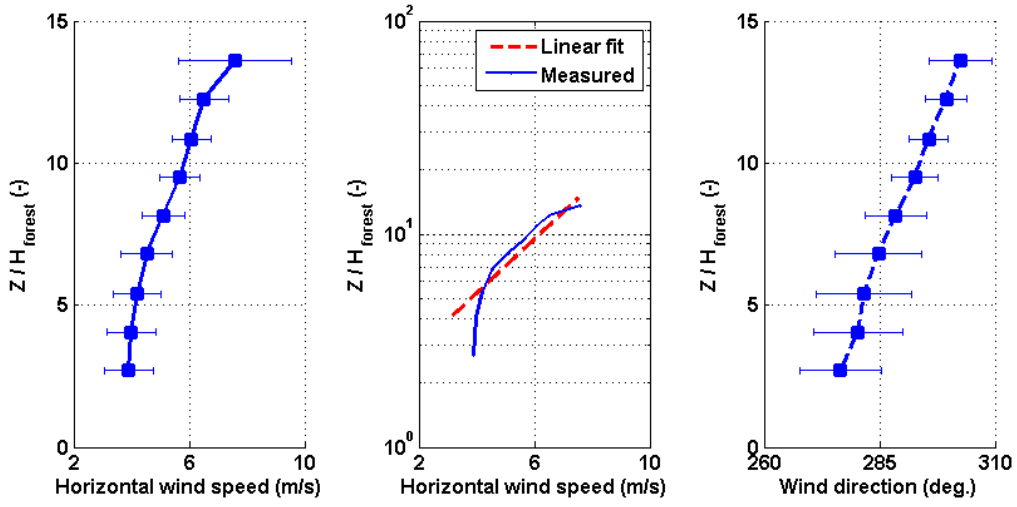

Fig. 5 Vertical profiles of wind speed and direction at the position "1" that is shown in Fig. 2b, a) wind speed, b) wind speed on semi-log scale, and c) wind direction.

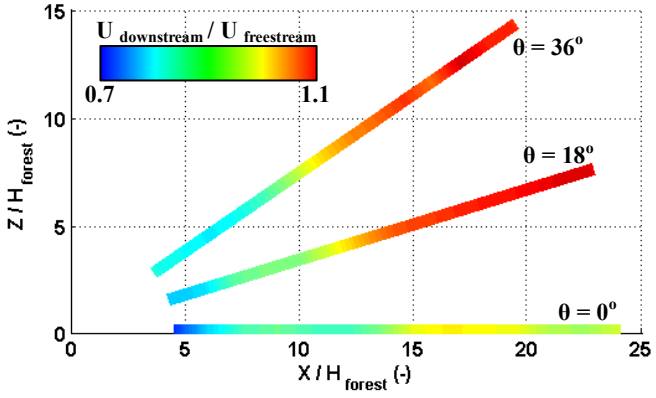

(a)

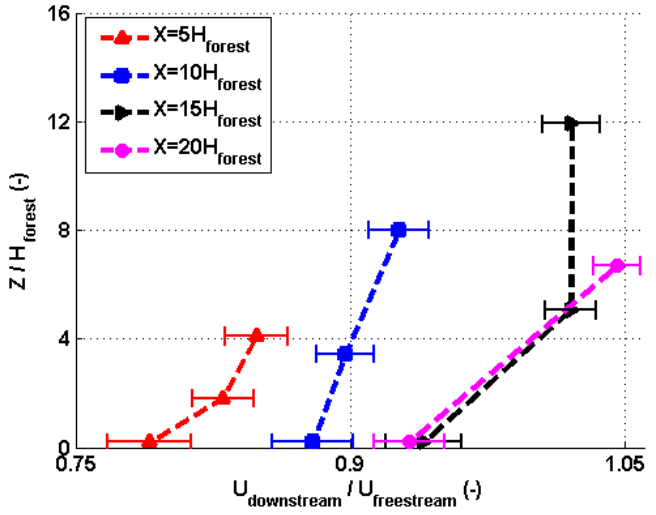

(b)

Fig. 6 Wind speed downstream of forest, a) wind speeds along beams of elevation angles 0°, 18°, 36°, and b) vertical profiles of wind speed at positions X= 5, 10, 15 and 20H_{forest} downstream of the forest.

It is observed that on beams with elevation angles of 18° and 36°, the wind speed approaches the freestream wind speed downstream of 12H_{forest}, whereas along the horizontal beam (elevation angle of 0°) shows a slower recovery, and even downstream of 25H_{forest} the wind speeds are lower than the freestream wind speed. Fig. 6b shows vertical profiles of the wind speed that are determined from the elevation scans shown in Fig. 6a; the profiles are 5, 10, 15 and 20H_{forest} downstream of the forest. The turbines downstream of the forest have a hub height of 4H_{forest}. Up to 20% deficit in wind speed adjacent to the ground and 15% at 4H_{forest} above ground level are measured at X=5H_{forest} downstream of the forest. The measured deficits in wind speed at height of 4H_{forest} are approximately equal at X=15H_{forest} and X=20H_{forest}, indicating that the recovery in wind speed at hub height occurs upstream of X=15H_{forest}. The measurement at X=10H_{forest} shows that the impact of the forest extends, at least, as high as Z=8H_{forest} at this downstream position.

Fig. 7 shows the turbulence intensities in the freestream, Fig. 7a, relative to position "1" in Fig. 2a and downstream of the forest, Fig. 7b, relative to position "2" in Fig. 2a. The turbulence intensities are higher downstream of the forest. The measurements along the horizontal beam (elevation angle θ=0°) show up to 25% increase in the turbulence intensity immediately downstream of the forest and a monotonic decay in turbulence as the flow evolves downstream. However the turbulence levels decrease more rapidly at higher heights. The turbulence intensity is the same as the freestream turbulence intensity at X=12H_{forest} and X=18H_{forest} at heights of Z=6H_{forest} and Z=10H_{forest}, respectively. With wind from the west the wind turbines with hub heights of 4H_{forest} are located at X=33H_{forest} (660m) downstream of the forest.

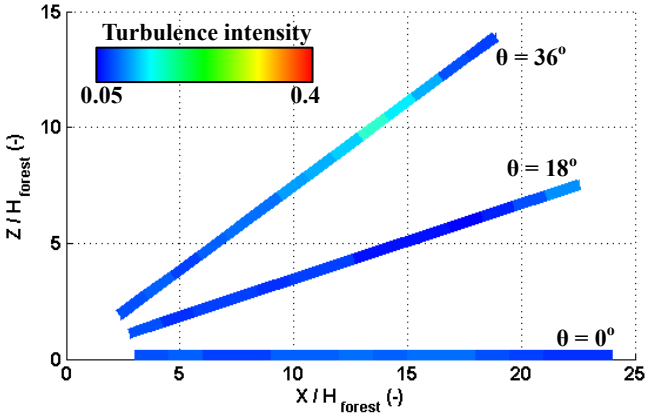

(a)

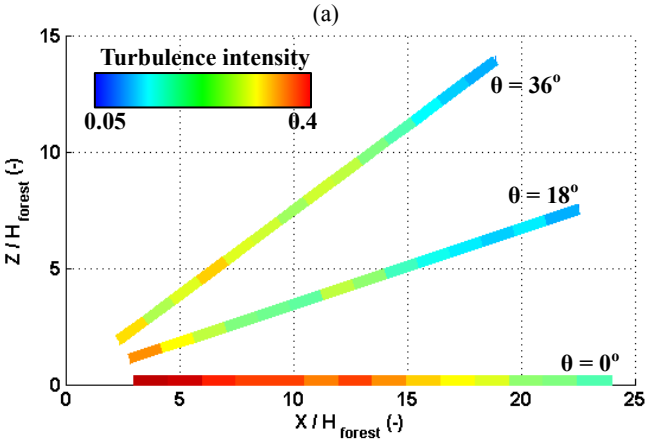

(b)

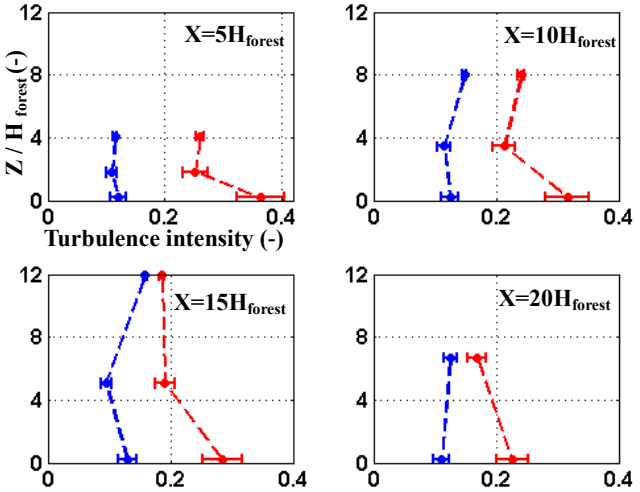

(c)

Fig. 7 Turbulence intensity upstream and downstream of forest, a) turbulence intensity in the freestream along beams of elevation angles 0°, 18°, 36°, b) turbulence intensity downstream of the forest along beams of elevation angles 0°, 18°, 36°, and c) vertical profiles of turbulence intensity in the freestream and downstream of the forest at X=5, 10, 15 and 20H_{forest}; red is downstream of the forest and blue is in the freestream.

The measurements show elevated levels of turbulence up to 12% at hub height at X=12H_{forest}. Fig. 7c shows vertical profiles of the turbulence intensity measured in the freestream, and downstream of the forest. The error bars show the expected range of turbulence intensity, over the range of degree of anisotropy, as discussed

above. Both measurements in the freestream and downstream of the forest generally show elevated turbulence levels near the ground. The turbulence intensity in the freestream is below 15% at all measurement positions. However the turbulence intensities are up to 26% at $X=5H_{forest}$ downstream of the forest. The turbulence intensity decreases from 26% at $X=5H_{forest}$ to 19% at $X=20H_{forest}$ downstream of the forest. Comparing Fig. 6b and Fig. 7c it is observed that although wind speed is the same as the freestream at $X=15H_{forest}$ and $X=20H_{forest}$, the turbulence intensities at these downstream positions are above the freestream turbulence intensities.

Impact of forest on annual energy yield

As observed in Fig. 2b, WEA10 faces a flat fetch for wind directions from 240° to 280°. However over the same range of wind directions the incoming wind to turbines WEA12, WEA13 and WEA14 flows over the forest. The energy yield of turbines WEA10, WEA12, WEA13 and WEA14 for the year 2014 is examined in Fig. 8. In this assessment, the power generation at wind speeds above rated wind speed and during maintenance of any of the turbines are excluded.

The direction-wise AEY of each turbine in 10-degree bins, where bin refers to the range of wind directions over which the AEY is evaluated, for wind directions of 245°, 255°, 265° and 275° are shown in Fig. 8a. The direction-wise AEY's range from 63MWh to 95MWh. WEA10 that faces an unforested flat fetch has the highest energy yield. Over the 240° to 280° range of wind directions WEA12, WEA13 and WEA14 have power deficits of 38.9MWh, 73.5MWh and 89.0MWh, respectively compared to WEA10. For a feed-in-tariff of 0.09EUR/kWh, these power deficits translate into yearly loss in income of 18100EUR.

Fig. 8b shows the power production of turbines WEA12, WEA13 and WEA14 normalised by the power of turbine WEA10. WEA14 has the largest power deficit over the range of wind directions with deficits as large as 30%. The distance to forest edge and the upstream extent of forest differs for the turbines, as a function of wind direction. Nevertheless, as observed in Fig. 2, the location for WEA14 is the most unfavourable, as this turbine is closest to the forest and the turbine is impacted by the forest over the whole range of wind directions. The power deficits are smaller for WEA13 and WEA12, as they are more distant from the forest. The distance to the forest edge and the upstream extent of the forest relative to WEA14 are shown in Fig. 8c and Fig. 8d, respectively. The distance to the forest edge determines how far upstream the elevated turbulence levels start to decay, and the upstream extent of forest determines how far upstream the forest-affected flow is. The distance to the forest edge, Fig. 8c, decreases monotonically from $45H_{forest}$ (900m) at 240° to $35H_{forest}$ (633m) at 280°, although the upstream extent of forest, Fig. 8d, increases from $100H_{forest}$ (2km) at 260° to $300H_{forest}$ (6km) at 270°. For the largest power deficit of 30% for WEA14, the upstream extent of the forest is $240H_{forest}$ (4.8km) and the distance to forest is $33H_{forest}$ (660m).

As can be seen from the wind rose at the site of Wind Farm 1, Fig. 3, the range of wind directions shown in Fig. 8 have the highest occurrence of 27%. Considering the wind rose, the average power deficits of WEA12, WEA13 and WEA14, shown in Fig. 8, represents a 1% loss of AEY of the whole wind farm.

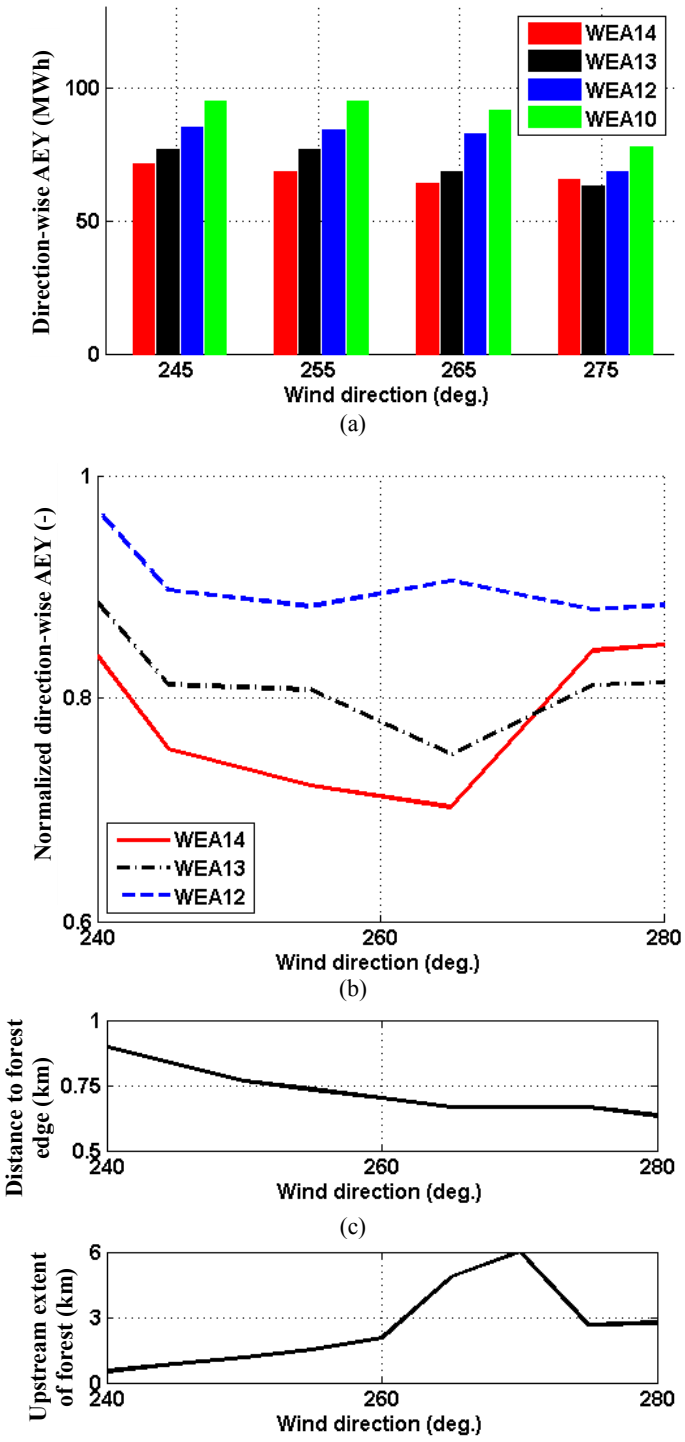

Fig. 8 a) Direction-wise AEY of wind turbines WEA10, WEA12, WEA13 and WEA14, b) Direction-wise AEY of wind turbines WEA12, WEA13 and WEA14, normalised by AEY of WEA10, c) upstream distance from the forest edge to the turbine WEA14 as a function of wind direction, and d) streamwise extent of forest upstream of turbine WEA14 as a function of wind direction.

Impact of forest on wake losses in wind farms

The impact of forests on the wake losses within wind farms is examined in Fig. 9. As wakes are characterised by a deficit in wind speed and elevated levels of turbulence, both of which are seen in the measurements above to be features of the flow downstream of forests, this impact is relevant for the further development of onshore wind farms. For this assessment, the one year long power generation of the wind turbines at Wind Farm 1, which is in flat

forested terrain, and Wind Farm 2, which is in flat unforested terrain, are assessed. From the 10-degree bin bucketed energy yields, Fig. 9 shows the decrease in the energy yield, that is wake loss, between turbine pairs [I, J], where (i) turbine I is in the wake of turbine J, or vice versa, and (ii) the turbine pair is separated less than 7D with no wake generating turbine within a distance of 10D from the turbine pair. Overall it can be seen in Fig. 9, that as the separation distance between wind turbine pairs increases the wake losses decreases. Indeed for the wind turbine pairs [7, 8] and [8, 9] in unforested terrain there is a 55% wake loss for a turbine separation of 3.5D, whereas the wake losses are 20% for the turbine pair [3, 5] with a separation distance of 6.5D in forested terrain. It can also be seen that for a given separation distance, the wake losses are larger in the unforested terrain compared to the forested terrain. As forests result in elevated turbulence levels, the higher mixing rates in the wake result in a faster recovery in the wind speeds, and therefore a smaller wake loss.

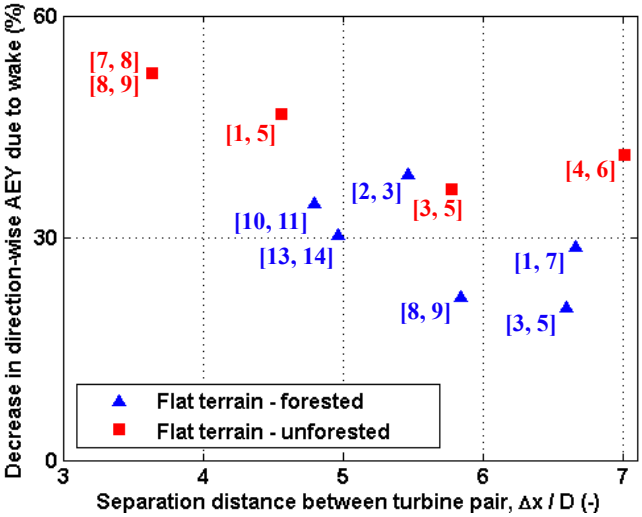

Fig. 9 Power deficit caused by the wake from upstream turbine.

CONCLUSIONS

In this work the impact of forests on the wind flow field and turbine performance are investigated. Measurements of wind speed and turbulence intensity are made in a wind farm in flat-forested terrain using a 3D scanning LiDAR. Turbulence measurements are based on the measured LOS wind speed and are corrected for the expected range of turbulence anisotropy. The measurements at hub height show a 15% deficit in wind speed $5H_{forest}$ downstream of the forest; this deficit decreases further downstream and is absent $15H_{forest}$ downstream of the forest. On the other hand, the elevated turbulence levels immediately downstream of the forest do not recover to the freestream turbulence level even at $20H_{forest}$ downstream of the forest. An assessment of the long-term SCADA data shows that there is up to 30% deficit in the direction-wise annual energy yield for wind turbines downstream of the forest, compared to a wind turbine with flat unforested fetch. Although deficits in wind speed and elevated turbulence levels due to forests are shown to have an adverse impact on power generation, wake losses are observed to be lower in forested terrain compared to unforested terrain. The smaller wake losses are attributed to higher mixing and faster recovery due to the elevated turbulence levels downstream of the forest.

ACKNOWLEDGEMENTS

The financial support of BKW FMB Energie AG and EOS Holding SA are gratefully acknowledged. PNE wind AG and EOS Wind Deutschland GmbH are kindly acknowledged for permission to access their respective wind farms. We also gratefully acknowledge the cooperation of Gregor Gloystein of EOS Wind Deutschland GmbH.

REFERENCES

[1] Global Wind Energy Council, 2014, "*Global Wind Statistics 2014*", Belgium.
[2] Ministry of Agriculture, Forestry and Fisheries, 2013, "*Annual Report on Forest and Forestry in Japan,*" Japan.
[3] http://www.demographia.com/db-metro-japan1965.htm
[4] Singh, A., Wolff, F., Chokani, N., Abhari, R. S., 2013, "*Optimizing Synergy of Utility-Scale Wind and Pumped-Hydro Storage*," IGTI Turbo Expo, San Antonio.
[5] Pedersen, H. S., Langreder, W., 2007, "Forest-added Turbulence: a Parametric Study on Turbulence Intensity in and around Forests," *Journal of Physics: Conference Series*, 75, 012062.
[6] Dellwik, E., Bingoel, F., Mann, J., 2013, "Flow Distortion at a Dense Forest Edge," *Royal Meteorological Society*, 140, pp. 676-686.
[7] Mann, J., Dellwik, E., 2014, "Sudden Distortion of Turbulence at a Forest Edge," *Journal of Physics: Conference Series*, 524, 012103.
[8] Vickers, D., Thomas, C. K., 2013, "Some Aspects of the Turbulence Kinetic Energy and Fluxes above and beneath a Tall Open Pine Forest Canopy," *Agricultural and Forest Meteorology*, 181, pp. 143-151.
[9] Segalini, A., Fransson, J. H. M., Alfredsson, P. H., 2013, "Scaling Laws in Canopy Flows: a Wind-Tunnel Analysis," *Boundary-Layer Meteorology*, 148, pp. 269-283.
[10] Dupont, S., Brunet, Y., 2009, "Coherent Structures in Canopy Edge Flow: a Large-Eddy Simulation Study," *Journal of Fluid Mechanics*, 630, pp. 93-128.
[11] Frank, C., Ruck, B., 2008, "Numerical Study of the Airflow over Forest Clearings," *Forestry*, 81, pp. 259-277.
[12] Odemark, Y., Segalini, A., 2012, "The Effects of a Model Forest Canopy on the Outputs of a Wind Turbine Model," *Jounrnal of Physics: Conference Series*, 555, 012079.
[13] Gottschall, J., Lindeloew-Marsden, P., Courtney, M., 2009, "*Executive Summary of Key Test Results for SgurrEnergy Galion*," Riso DTU, Roskilde, Denmark.
[14] IEC61400-1, 2005, "*Wind turbines – Part I: Design Requirements*," International Electrotechnical Commission.
[15] Mansour, M., Schmid, T., Chokani, N., Abhari, R. S., 2014, "Power Curve Assessment of a 2MW Wind Turbine Located in Complex Terrain," *European Wind Energy Conference*, Barcelona.
[16] Ettlin, K, Mansour, M., Subramanian, B., Costa, D., Chokani, N., Abhari, R. S., 2013, "*Near-Wake Measurements in an Offshore Reference Field Using a Kite-Borne Aerodynamic-Probe-System*," European Wind Energy Association Annual Event 2013, Vienna.
[17] Panofsky, H. A., Dutton, J. A., 1984, "*Atmospheric Turbulence*," Wiley, New York.
[18] Crespo, A., Hernandez, J., 1995, "Turbulence Characteristics in Wind-Turbine Wakes," *Journal of Wind Engineering and Industrial Aerodynamics*, 61, pp. 78-85.
[19] Cleijne, J. W., 1993, "*Results of Sexbierum Wind Farm: Single Wake Measurements*," TNO, Apeldoorn.
[20] Stull, R. B., 2009, "*An Introduction to Boundary Layer Meteorology*," Springer, Vancouver.
[21] Eser, P., Singh, A., Chokani, N., Abhari, R. S., 2015, "*High Resolution Simulations of Increased Renewable Penetration on Central European Transmission Grid*," IEEE PES General Meeting, Denver.